A Low-Field Portable Nuclear Magnetic Resonance (NMR) Microfluidic Flowmeter

Aydin, Eren; Makinwa, Kofi A.A.

A LOW-FIELD PORTABLE NUCLEAR MAGNETIC RESONANCE (NMR) MICROFLUIDIC FLOWMETER

Eren Aydin[1], and Kofi A.A. Makinwa[1]
[1]Electronic Instrumentation Laboratory, Delft University of Technology, Delft, The Netherlands

ABSTRACT

This paper presents a portable and contactless microfluidic flowmeter based on the Nuclear Magnetic Resonance (NMR) principle, which can measure flow rates up to 2.7 ml/min with ±16 µl/min (±0.6% full-scale) error. It consists of a millimeter-size RF coil wound around a microfluidic channel, custom readout electronics and a 0.5 T permanent magnet with 50 ppm inhomogeneity. To our knowledge, this is the first reported low-field NMR microfluidic flowmeter.

KEYWORDS

NMR, flowmeter, microfluidics, analog front-end, low noise transceiver.

INTRODUCTION

Precise control and sensing of flow rates is required in many lab-on-a-chip applications [1]. MEMS thermal flow sensors are widely used due to their simplicity, scalability, low-power, high-sensitivity and practicality [2]. MEMS Coriolis flow sensors are gaining popularity due to their fluid-independent sensing capability and simple calibration [3]. However, both types of sensors require physical contact with the fluid, complicating the fluidic setup, changing the flow profile and causing pressure drops. Moreover, such sensors may be damaged by corrosive or scalding liquids.

Ultrasonic [4] and electromagnetic [5] flowmeters are contactless. However, their operation is highly dependent on the specific acoustic or electrical properties of the fluid, respectively. Moreover, they are not compatible with the narrow tubes (< 1mm diameter) that are often used in microfluidic applications [6]. In contrast, Nuclear Magnetic Resonance (NMR) flowmeters are also contactless, but can be used with a wide variety of fluids, and can also be used to analyze fluid composition. The latter is especially useful in biomedical applications.

However, current NMR flowmeters can only measure high flow rates (hundreds of l/min) and are quite bulky and expensive [7], [8]. Although some miniature NMR devices based on low-field permanent magnets and CMOS or PCB-based electronics have been reported [9]–[12], these were intended for sample analysis and not for flow sensing.

This paper proposes a portable NMR flowmeter that can measure flow rates as low as a few tens of µl/min. The paper is organized as follows. First, the basic principles of NMR-based flow sensing will be explained. Then, the custom analog readout and the test setup will be described. After that, the measurement results are presented, and followed by some conclusions.

THEORETICAL BACKGROUND

The term NMR refers to the resonant interaction between an RF magnetic field (B₁) and nuclei in the presence of a static magnetic field (B₀). The randomly distributed magnetic moments of the protons in a sample will align themselves with the external field (Figure 1). However, this alignment will be disturbed by an external RF field (B₁) that is perpendicular to B₀ (Figure 1-c) at the so-called Larmor frequency (f_{Larmor}), given by:

$$f_{Larmor} = \gamma B_0 \qquad (1)$$

where γ is the gyromagnetic ratio and is a material-dependent parameter. For example, γ is equal to 42.58 MHz/T for hydrogen. The duration of the RF field determines the angle of misalignment, which should be 90° for maximum effect (Figure 1-d). When the RF field is turned off, the magnetic moments will re-align themselves with B₀ and emit an NMR signal (Figure 1-e). The decay time constant of the NMR signal depends on the spin-spin relaxation (T₂) mechanism, which is sample-dependent.
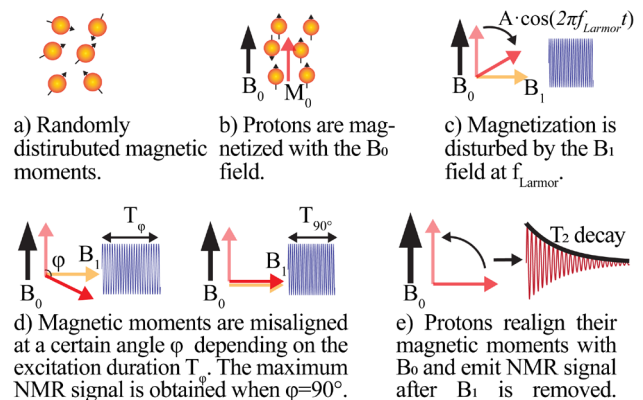

a) Randomly distributed magnetic moments.

b) Protons are magnetized with the B₀ field.

c) Magnetization is disturbed by the B₁ field at f_{Larmor}.

d) Magnetic moments are misaligned at a certain angle φ depending on the excitation duration $T_φ$. The maximum NMR signal is obtained when φ=90°.

e) Protons realign their magnetic moments with B₀ and emit NMR signal after B₁ is removed.

Figure 1: Illustration of the NMR Principle.

Inhomogeneity in the B₀ field will cause different spins to have different Larmor frequencies, decreasing the coherence of the NMR signal, and shortening the decay time constant (T₂*). One way around this problem is the use of spin-echo measurements. After a $T_{90°}$ pulse, the application of a $T_{180°}$ pulse will invert the magnetic moments, causing the decaying spins to gradually re-align and emit a so-called echo signal [13]. As shown in Figure 2, Carr and Purcell [14] proposed a pulse sequence that exploits this spin-echo phenomenon. It consists of a $T_{90°}$ pulse followed by a train of $T_{180°}$ pulses. The interval between the $T_{180°}$ pulses is twice the interval between the $T_{90°}$ and the first $T_{180°}$ pulse [14]. The T₂ decay can then be accurately estimated from the peaks of the echo signals.

Carr-Purcell pulse sequences can also be used for flow measurement [7]. In the absence of flow, the usual exponential T₂ decay will occur. In the presence of flow, however, the decay will be faster as the magnetized fluid volume move away from the RF detection coil. The exponential decay will thus be modulated by an additional flow-rate dependent decay *f(t)*, which can be obtained by normalizing the measured decay with the no-flow decay (T₂ normalization) [7], [8]. This normalization ensures that *f(t)* is fluid independent. An illustrative plot of the resulting signals at different flow rates is shown in Figure 3.
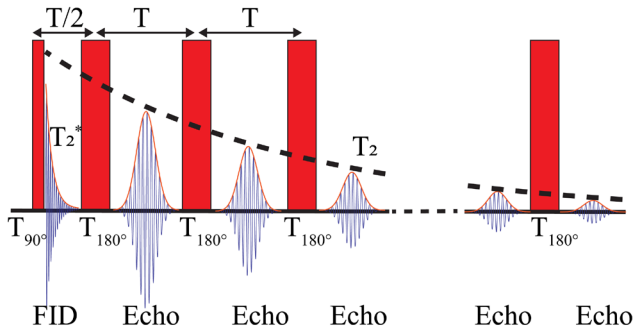
Figure 2: Illustration of Carr-Purcell pulse sequences, the red rectangles represent the RF excitation moments.
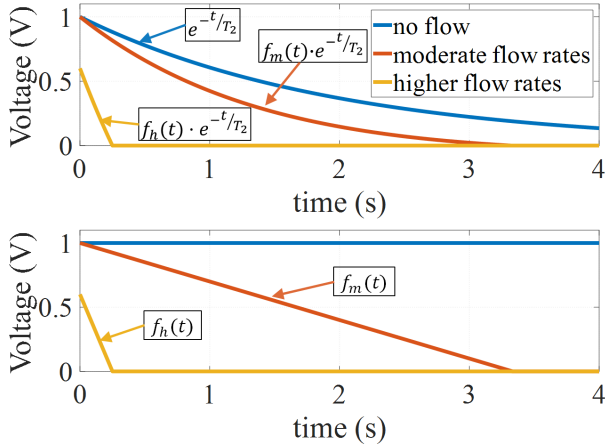

Figure 3: Effect of flow on T_2 decay (top: T_2 decay, bottom: T_2 normalized signal $f(t)$). The peak value of $f(t)$ decreases with flow rate since the shorter exposure to the B_0 field results in the magnetization of fewer molecules.

The average normalized slope of $f_n(t)$, where n indicates the flow rate, is then proportional to the flow rate. It can be determined by dividing the maximum value of $f_n(t)$ by the area under the $f_n(t)$ curve:

$$normalized\ slope_n = \frac{\max(f_n(t))}{\int_0^\infty f_n(t)\,dt} \quad (2)$$

ANALOG FRONT-END AND SIGNAL ACQUISITION

An NMR system can be regarded as an AM radio transceiver that operates at the Larmor frequency. The B_1 field is applied to the sample by an RF coil, which is also used to pick up the NMR signal. A transmitter drives the coil, and a receiver detects, amplifies, and demodulates the NMR signal. This is then digitized and processed to determine the T_2 decay.

The circuit implementation of the proposed NMR system is shown in Figure 4. To optimally reject external interference, the RF coil is embedded in a fully differential matching network. Its resonance frequency is set to the expected Larmor frequency (~21.71 MHz) by tuning C_t, while capacitors C_m are used to achieve 50 Ω matching, and thus optimize the power transfer to the RF transceiver. A balun (Minicircuits, 1-6T-KK81+) is used to generate the single-ended signal required by the receiver.

To minimize truncation of the initial FID and echo signals, the RF coil must be rapidly switched between the transmitter and the receiver. This is done by TX/RX switches, which are realized by anti-series PIN diodes (BAP65-03) that enable switching times of < 10 μs (limited by coil ringing). The switches also isolate the sensitive receiver from the large amplitude (10 V_{pp} @ $f_{excitation}$) excitation signals.

Since the amplitude of the NMR signal at the coil output is in the micro-volt range, the first stage of the receiver is an LNA (Minicircuits, LHA-13LN+) with 1.1 dB NF and 22 dB gain. Depending on the diameter of the microfluidic tubing, the size of the RF coil, and hence its output amplitude can vary significantly. To prevent receiver saturation, a variable gain amplifier (VGA) (AD8331) is used as the second amplification stage. In this work, two different coils were used, enabling sample volumes of 3 μL and 27 μL, respectively.

An IQ demodulation scheme is used to accommodate the ill-defined phase difference between the NMR signal and the demodulation signal. Active mixers (AD831) down-convert the NMR signal to 50kHz with the help of f_{LO_I} and f_{LO_Q} signals (≈21.66 MHz). After digitization, the final down-conversion of the resulting I_{out} and Q_{out} signals to DC can then be performed entirely in the digital domain. This approach effectively suppresses the offset and drift of the analog front-end.

The digitization of the receiver output and the generation of timing signals is done by a data acquisition board (NI-USB6363) with 16-bit ADCs with a 1 MS/s sampling rate. To ensure that their quantization noise does not limit system resolution, an IF amplifier (LTC1250) is used to first boost the I and Q signals by 30 dB. The digitized signals are then applied to a digital bandpass filter with a 50 kHz center frequency and a 40 kHz bandwidth, which improves their SNR and removes DC offset. The filtered I_{filt} and Q_{filt} signals are then vectorially combined to generate the final NMR signal.

Ideally, the peaks of the echo signal should occur exactly half-way between two consecutive $T_{180°}$ pulses in the Carr-Purcell pulse sequence. Due to the narrow-band characteristics of the receiver, however, the NMR signals are delayed by about 50 μs. To avoid the noise penalty incurred by traditional peak detectors, the peak amplitudes were computed by averaging the NMR signal over a 100 μs window with 50 μs delay.

MEASUREMENT SETUP AND RESULTS

The fluidic connections and electronic interface of the test setup are shown in Figure 5. A pressurized falcon tube is used to maintain a constant pressure of 2.5 bars, while the flow rate is set by a mass flow controller (Bronkhorst mini-CORIFLOW), resulting in flow rates up to 2.67 ml/min. At this rate, the calculated Reynolds number is 79 [15], which corresponds to laminar flow. For the experiments without flow, the flow controller and the pressurized falcon were removed to simplify the setup. For the experiments, two different coils (coil 1 and coil 2) were employed. Their dimensions and pulse sequence parameters are given in Table 1 and Table 2, respectively.
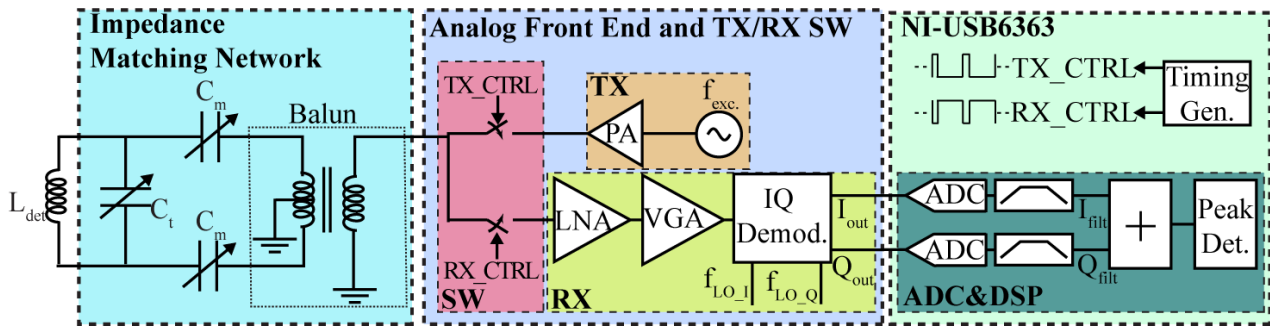
Figure 4: Circuit implementation of the proposed NMR system.

The measurement setup is shown in Figure 6. To shield it from interference, the analog front-end is placed in a grounded metal box. The Larmor frequency of the magnet varies between 21.65 MHz to 21.75 MHz due to the B_0 drift caused by temperature variations. To compensate for this, the excitation and demodulation signal frequencies are tuned before each experiment.

Table 1: Coil dimensions: D, L, and N represent the diameter, length, and the number of windings respectively.

Coil No	D (mm)	L (mm)	N
1	5	6	7
2	2.2	6	7

Table 2: Pulse sequence parameters: T_{pulse} and N_{pulse} represent the period and number of 180° pulses.

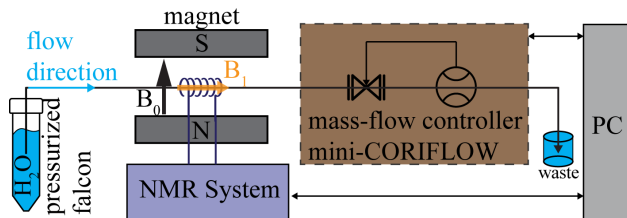| Coil No	$T_{90°}$ (µs)	$T_{180°}$ (µs)	T_{pulse} (ms)	N_{pulse}
1	45	90	2	500
2	30	60	2	2000

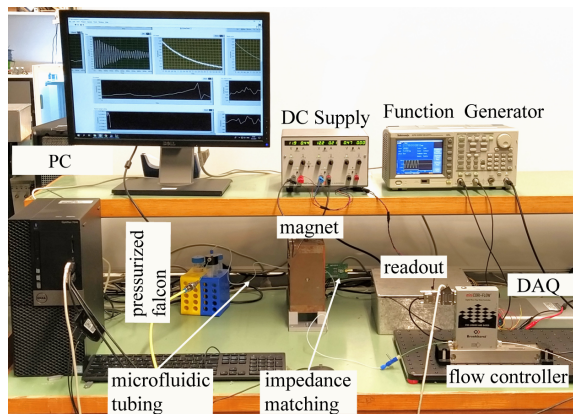Figure 5: Illustration of the test setup.

Figure 6: The photograph of the test setup.

In the absence of flow, T_2 decays obtained with three different samples are shown in Figure 7: water, sunflower oil, and a mixture of water and sunflower oil. For the water sample, the T_2 decay is exponential with a 2.05 s time-constant, while that of the oil sample is a combination of

two exponentials with 200 ms and 60 ms time constants. As expected, the decay of the mixture is a superposition of these decays, which depends on the oil to water ratio.
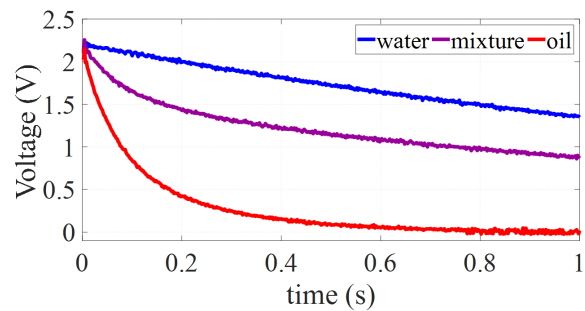

Figure 7: T_2 decays obtained with coil 1 from different 27µL samples with a 2.4mm (inner diameter) tube.

The NMR signals obtained for flow rates varying from 0 to 2.67 ml/min are shown in Figure 8. The resulting decays were then T_2 normalized, as shown in Figure 9, and de-noised by fitting them to the generalized decay function shown below, where a, b and c are fitting parameters:

$$f(t) = a \cdot e^{-(b \cdot t)^c} \qquad (3)$$

Finally, the average normalized slopes were determined from Eq. 2.

As shown in Figure 10 (straight lines), the calculated slopes exhibit a near-linear relationship with flow rate. Applying a first-order polynomial fit results in a full-scale (FS) error of ±2%, Figure 10 (dashed lines). With a second-order polynomial, the error can be reduced to ±0.6% (±16 µl/min), which is comparable with that of commercially available flowmeters [16].
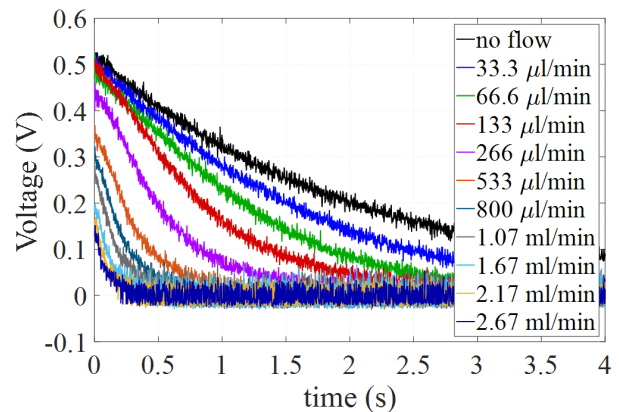

Figure 8: NMR signals obtained with coil 2 and standard microfluidic tubing (1.6 mm outer and 0.8 mm inner diameter) for flow rates varying from 0 to 2.67 ml/min.
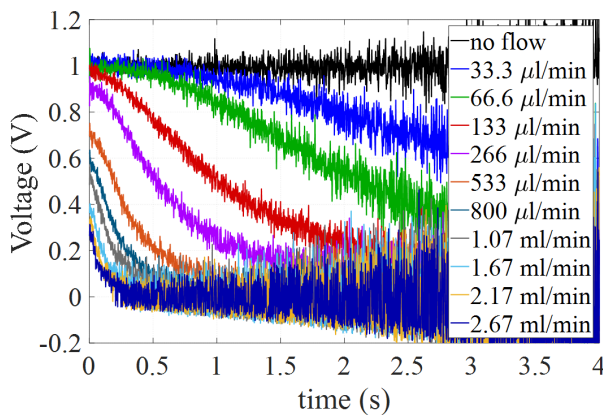
1022

Figure 9: T₂-normalized NMR signals with various flow rates from 0 to 2.67 ml/min.

The input-referred noise density (< 1 nV/√Hz) of the proposed NMR system is comparable to that of other miniature NMR systems [9], [11], and so it can be used to obtain T₂ decays from sample volumes ranging from 27 μL and 3 μL. Although the minimum sample volume is limited by practical constraints on the minimum coil dimensions; reliable NMR signals could be obtained from sample volumes as small as 1 μL. This is comparable with the performance of other miniature NMR systems, which were tested with 7 μL samples [9], [11]. However, our system is the first to also demonstrate flow-sensing capability.
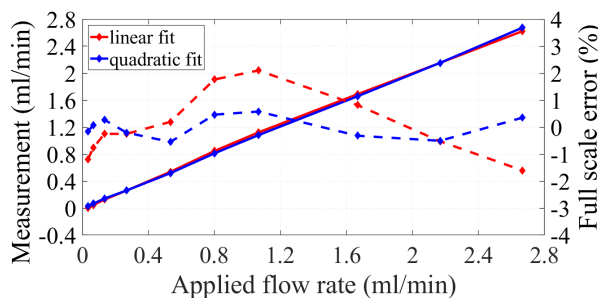

Figure 10: Measured flow rate (left y-axis, straight lines) and full-scale error (right y-axis, dashed lines) with respect to the applied flow rate.

CONCLUSION

In this paper, the first portable NMR microfluidic flowmeter has been presented. It can measure flow rates up to 2.7 ml/min with ±0.6% (full-scale) accuracy. The actual flow range can be flexibly adjusted by appropriately changing the coil and tubing sizes. The proposed system demonstrates that NMR can be simultaneously used for non-contact flow measurement and for sample analysis. Overall, this work is the first step towards portable NMR microfluidic flowmeters that can be used in both academic and industrial applications.

ACKNOWLEDGEMENTS

REFERENCES

[1] H. A. Stone, A. D. Stroock, and A. Ajdari, "Engineering flows in small devices: Microfluidics toward a lab-on-a-chip," *Annu. Rev. Fluid Mech.*, vol. 36, no. 1, pp. 381–411, Jan. 2004.

[2] J. T. W. Kuo, L. Yu, and E. Meng, "Micromachined Thermal Flow Sensors—A Review," *Micromachines*, vol. 3, no. 3, pp. 550–573, Jul. 2012.

[3] A. C. De Oliveira *et al.*, "A MEMS Coriolis Mass Flow Sensor with 300 μg/h/√Hz Resolution and ±0.8mg/h Zero Stability," in *IEEE ISSCC*, Feb. 2021, pp. 84–86.

[4] Y. Chen *et al.*, "Continuous ultrasonic flow measurement for aerospace small pipelines," *Ultrasonics*, vol. 109, p. 106260, Jan. 2021.

[5] L. Ge *et al.*, "Study on a New Electromagnetic Flow Measurement Technology Based on Differential Correlation Detection," *Sensors*, vol. 20, no. 9, pp. 2489, Apr. 2020.

[6] Y. Yu and G. Zong, "Note: Ultrasonic liquid flow meter for small pipes," *Rev. Sci. Instrum.*, vol. 83, no. 2, p. 026107, Feb. 2012.

[7] T. M. Osán *et al.*, "Fast measurements of average flow velocity by Low-Field 1H NMR," *J. Magn. Reson.*, vol. 209, no. 2, pp. 116–122, Apr. 2011.

[8] A. M. Bilgic *et al.*, "Multiphase flow metering with nuclear magnetic resonance," *Tech. Mess.*, vol. 82, no. 11, pp. 539–548, Nov. 2015.

[9] K.-M. Lei, P.-I. Mak, M.-K. Law, and R. P. Martins, "A μNMR CMOS Transceiver Using a Butterfly-Coil Input for Integration With a Digital Microfluidic Device Inside a Portable Magnet," *IEEE JSSC*, vol. 51, no. 10, pp. 2274–2286, Oct. 2016.

[10] D. Ariando, C. Chen, M. Greer, and S. Mandal, "An autonomous, highly portable NMR spectrometer based on a low-cost System-on-Chip (SoC)," *J. Magn. Reson.*, vol. 299, pp. 74–92, Feb. 2019.

[11] S. Hong and N. Sun, "A Portable NMR System with 50-kHz IF, 10-us Dead Time, and Frequency Tracking," in *IEEE VLSI*, Jun. 2020.

[12] H. Burkle *et al.*, "A High Voltage CMOS Transceiver for Low-Field NMR with a Maximum Output Current of 1.4 A pp," in *IEEE ISCAS* Sep. 2020.

[13] E. L. Hahn, "Spin echoes," *Phys. Rev.*, vol. 80, no. 4, pp. 580–594, Nov. 1950.

[14] H. Y. Carr and E. M. Purcell, "Effects of diffusion on free precession in nuclear magnetic resonance experiments," *Phys. Rev.*, vol. 94, no. 3, pp. 630–638, May 1954.

[15] J. H. Spurk and N. Aksel, *Fluid Mechanics*. Cham: Springer International Publishing, 2020.

[16] "Elveflow product catalog - Elveflow." https://www.elveflow.com/elveflow-community/download/elveflow-product-catalog-dedicated-to-microfluidics/ (accessed Feb. 25, 2021).

CONTACT

*E. Aydin, tel:+31(0)15279081; e.aydin@tudelft.nl